Chemical Science

ROYAL SOCIETY OF CHEMISTRY

EDGE ARTICLE

View Article Online
View Journal | View Issue

Check for updates

Cite this: *Chem. Sci.*, 2020, **11**, 9513

All publication charges for this article have been paid for by the Royal Society of Chemistry

Received 20th July 2020
Accepted 13th August 2020

DOI: 10.1039/d0sc03955a

rsc.li/chemical-science

Spatial confinement alters the ultrafast photoisomerization dynamics of azobenzenes†

Christopher J. Otolski,‡[a] A. Mohan Raj,[b] Vaidhyanathan Ramamurthy *[b] and Christopher G. Elles *[a]

Ultrafast transient absorption spectroscopy reveals new excited-state dynamics following excitation of *trans*-azobenzene (*t*-Az) and several alkyl-substituted *t*-Az derivatives encapsulated in a water-soluble supramolecular host–guest complex. Encapsulation increases the excited-state lifetimes and alters the yields of the *trans* → *cis* photoisomerization reaction compared with solution. Kinetic modeling of the transient spectra for unsubstituted *t*-Az following nπ* and ππ* excitation reveals steric trapping of excited-state species, as well as an adiabatic excited-state *trans* → *cis* isomerization pathway for confined molecules that is not observed in solution. Analysis of the transient spectra following ππ* excitation for a series of 4-alkyl and 4,4′-dialkyl substituted *t*-Az molecules suggests that additional crowding due to lengthening of the alkyl tails results in deeper trapping of the excited-state species, including distorted *trans* and *cis* structures. The variation of the dynamics due to crowding in the confined environment provides new evidence to explain the violation of Kasha's rule for nπ* and ππ* excitation of azobenzenes based on competition between in-plane inversion and out-of-plane rotation channels.

1 Introduction

Many important photoisomerization reactions take place in the confined environment of a protein or solid-state material.[1–3] Steric restrictions often play a key role in these reactions by inhibiting large amplitude motions of the atoms and stabilizing, or destabilizing, specific structures along the reaction path. For example, crowding facilitates the primary steps responsible for vision and phototaxy by steering the photoisomerization of protein-bound chromophores toward the desired outcome.[4–7] In contrast, confinement in a polymer matrix or nanoporous material often inhibits the reactions of photochromic molecules compared with solution.[8–10] Understanding how confinement affects the excited-state dynamics therefore promises new insight on the fundamental details of light-activated biological systems, and provides important guidance for designing new materials that preserve the efficiency of photochromic molecules in solid-state applications.

Azobenzenes are prototypical molecular switches that combine the benefits of relatively fast and efficient *trans* → *cis* photoisomerization with thermal *cis* → *trans* relaxation.[11–14] The photoisomerization dynamics of azobenzenes are particularly sensitive to the influence of a confined environment because of the different geometric requirements for the competing out-of-plane rotation and in-plane inversion pathways for isomerization around the N=N bond.[15–23] Even in solution, the relative importance of the rotation and inversion channels is not fully understood due to short (few ps or less) excited-state lifetimes and wavelength-dependent isomerization yields.[24–26] In fact, the different quantum yields following excitation to the $S_1(n\pi^*)$ and $S_2(\pi\pi^*)$ excited states is a defining feature of azobenzenes,[27,28] and a rare example of a reaction that violates the venerable Kasha–Vavilov rule.[29–31]

Given the influence of steric restrictions on photoisomerization, measuring the excited-state dynamics in a confined environment provides a sensitive probe of the reaction mechanism for azobenzenes. With that goal in mind, this paper examines the excited-state dynamics for a series of azobenzenes encapsulated in a supramolecular host–guest complex that restricts the motion of the phenyl rings around the central N=N bond.[32–35] Each self-assembled complex consists of a single molecule of azobenzene encapsulated in the hydrophobic cavity formed by two water-soluble 'octa-acid' (OA) host molecules (Fig. 1).[36–40] The photochemistry of geometric isomerization and bimolecular reactions in the OA_2 cavity have been

[a]*Department of Chemistry, University of Kansas, Lawrence, Kansas, USA. E-mail: elles@ku.edu*

[b]*Department of Chemistry, University of Miami, Coral Gables, Florida, USA. E-mail: murthy1@miami.edu*

† Electronic supplementary information (ESI) available: Additional ground-state spectra, transient absorption spectra, and species-associated spectra from kinetic fits to the data (PDF). See DOI: 10.1039/d0sc03955a

‡ Present address: Chemical Sciences and Engineering Division, Argonne National Laboratory, Lemont, Illinois, USA.

Open Access Article. Published on 24 August 2020. Downloaded on 4/19/2026 12:43:29 PM.
This article is licensed under a Creative Commons Attribution-NonCommercial 3.0 Unported Licence.

Open Access Article. Published on 24 August 2020. Downloaded on 4/19/2026 12:43:29 PM.
This article is licensed under a Creative Commons Attribution-NonCommercial 3.0 Unported Licence.

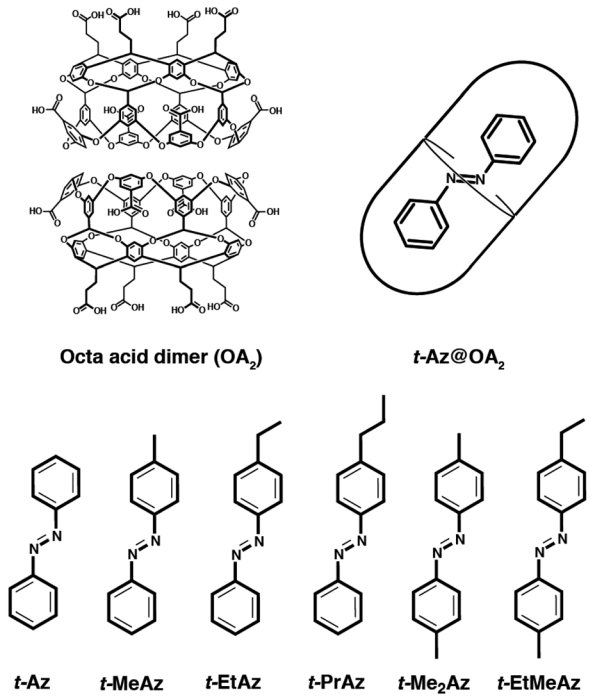

Fig. 1 Structures of the octa-acid dimer (OA_2) and the series of *trans*-azobenzenes. From left to right: azobenzene (Az), 4-methylazobenzene (MeAz), 4-ethylazobenzene (EtAz), 4-propylazobenzene (PrAz), 4,4′-dimethylazobenzene (Me_2Az), 4,4′-ethylmethylazobenzene (EtMeAz).

studied extensively using steady-state methods,[39] and we recently reported on the ultrafast photoisomerization dynamics of 4-propylstilbene and 4-propylazobenzene,[34] as well as a series of alkyl-substituted stilbenes with increasing size.[35] Interactions with the capsule directly influence the reaction and relaxation channels by distorting the ground- and excited-state potential energy surfaces of the confined molecule, providing a unique window on the reaction dynamics.

In this paper, we examine the role of crowding effects on the azo isomerization by comparing the excited-state dynamics of encapsulated *trans*-azobenzene (*t*-Az@OA_2) and several 4-alkyl- and 4,4′-dialkyl-substituted derivatives (Fig. 1). For unsubstituted *t*-Az, we compare the excited-state dynamics following $n\pi^*$ excitation at 470 nm and $\pi\pi^*$ excitation at 320 nm. These wavelength-dependent measurements reveal enhanced violation of Kasha's rule in the capsule compared with solution, including a new adiabatic excited-state isomerization channel that is not observed for the freely solvated molecule. We also compare the dynamics following $\pi\pi^*$ excitation across the series of alkyl-substituted compounds in the two environments. Increasing the alkyl-chain length changes the relative stability of the *trans* and *cis* isomers inside the capsule, and thus alters the photoisomerization yields compared with solution. Comparing the dynamics across the series of encapsulated compounds provides new insight on the role of steric interactions in tuning the excited-state dynamics, including the "trapping" of excited-state species that are not observed in solution.

2 Experimental details

Unsubstituted *t*-Az was purchased from Sigma-Aldrich and used as received. Octa acid (OA) and all of the alkyl-substituted *trans*-azobenzenes were synthesized as previously reported.[32,33,37] We form self-assembled complexes (guest@OA_2) by sonicating 2 equivalents of OA in pH = 8.9 borate buffer with 1 equivalent of azobenzene until the solution is transparent.[35,36,40] The transient absorption (TA) measurements for $n\pi^*$ excitation use an 8 mM solution of either *t*-Az in cyclohexane or mixed isomers of Az in OA_2 at photostationary state (PSS). We obtain PSS by continuously irradiating the sample of Az@OA_2 with a high-intensity 300 nm light-emitting diode to obtain a steady-state equilibrium between the two isomers. Comparing the absorption spectrum of the sample before and after each TA measurement confirms that the relative concentration of isomers remains unchanged throughout the experiment. The TA measurements for $\pi\pi^*$ excitation use either a 1 mM solution of the *trans* isomer of a compound dissolved in cyclohexane or a ~0.5 mM solution of the *trans* isomer inside the aqueous OA_2 capsule. We measure all TA spectra in a circularly translating quartz cuvette with a path length of 1 mm.

The TA measurements use the modified output of a regeneratively amplified Ti:sapphire laser (Legend Elite, Coherent) operating at 1 kHz. A portion of the 800 nm output of the laser is passed into an optical parametric amplifier (OPA) with two additional stages of nonlinear frequency conversion to generate pump pulses at either 470 or 320 nm. A CaF_2 prism pair compresses the pump pulses to a duration < 80 fs and a zero-order $\lambda/2$ wave plate sets the pump polarization to parallel or perpendicular orientation with respect to the probe. We focus the pump pulses into the sample with an energy of <1.2 μJ per pulse and diameter of ~200 μm. Broadband probe pulses covering the range 340–990 nm come from white-light continuum generation in a circularly translating CaF_2 crystal using the 1200 nm signal from a second, home-built OPA. We use a pair of parabolic mirrors to collimate, then focus the probe beam into the continuously translating sample, where the pump and probe beams overlap at a small crossing angle. After passing through the sample, a prism disperses the probe pulses onto a 256-element photodiode array for shot-to-shot detection. A synchronized chopper blocks every other pump pulse for active background subtraction, and we average 10^3 laser pulses per time delay for each spectrum. We continuously translate the sample in order to avoid accumulation of photoproduct in the laser focal volume. We measure TA spectra for both parallel and perpendicular polarization, then calculate the isotropic spectra, $\Delta A_{iso} = (\Delta A_{\parallel} + 2\Delta A_{\perp})/3$, in order to eliminate contributions from rotational reorientation.[41]

Independently, we measure the *trans* → *cis* photoisomerization quantum yields ($\Phi_{t\rightarrow c}$) for $\pi\pi^*$ excitation by monitoring the change in transmission of 320 nm laser pulses through a solution of the *trans* isomer in a static 1 mm cuvette.[42,43] In order to account for small shot-to-shot fluctuations of the laser, we use a 50% beam splitter to separate the UV laser light into signal and reference beams before the sample,

 This journal is © The Royal Society of Chemistry 2020

Open Access Article. Published on 24 August 2020. Downloaded on 4/19/2026 12:43:29 PM.
This article is licensed under a Creative Commons Attribution-NonCommercial 3.0 Unported Licence.

then simultaneously measure the intensity of the two beams with identical integrating photodiodes operating at 1 kHz. The transmission of the signal beam through the sample (1.5 mm beam diameter, 2.5 nJ per pulse incident energy) increases as a function of time due to the conversion from *trans* to *cis*. The change in absorption is proportional to the number of molecules that isomerize, because only the *trans* isomer has appreciable absorption at 320 nm. Thus, we calculate $\Phi_{t\rightarrow c}$ from the relative change in absorption as a function of time compared with the absolute absorption of the sample.

3 Results and analysis

3.1 Ground-state spectra and quantum yields

Fig. 2 shows the ground-state absorption spectra of *t*-Az in cyclohexane, *t*-Az@OA_2 in borate buffer, and adamantane@OA_2 in borate buffer. The *t*-Az spectrum has a strong ππ* absorption band near 320 nm and a weaker nπ* absorption band near 440 nm. The weaker band is also shown on an expanded scale for clarity. The spectrum of *t*-Az@OA_2 is very similar to that of the freely solvated molecule, except for an overlapping absorption band of OA_2 below 300 nm and a shift of the ππ* band to slightly longer wavelength. The spectrum of adamantane@OA_2 confirms that the band at 280 nm is due to the OA_2 capsule, because adamantane is transparent above 200 nm.[44]

In Fig. 3, we compare the ππ* absorption bands for the series of alkyl-substituted azobenzenes. All six molecules have similar spectra in cyclohexane, except for a slight shift to longer wavelength with the addition of one or two alkyl substituents. Similar to *t*-Az, most of the spectra shift further to the red upon encapsulation, but retain the same vibronic structure. However, the spectra for *t*-EtAz@OA_2 and *t*-PrAz@OA_2 clearly deviate from the others. The ππ* absorption bands for these two encapsulated compounds are shifted to higher energy and have significantly less vibronic structure, which is a signature of reduced conjugation and indicates a distorted, non-planar equilibrium geometry inside the OA_2 capsule.[35] The effect is not surprising for these two molecules, as they have the longest alkyl chains, and therefore experience the most crowding inside the capsule. Interestingly, the di-substituted compounds *t*-Me_2Az and *t*-EtMeAz retain their vibronic structure in the capsule, even though the total lengths of these two molecules are similar to *t*-EtAz and *t*-PrAz, respectively. The difference probably reflects better packing of the alkyl groups into the ends of the OA_2 capsule for the di-substituted compounds compared with the packing of the unmodified phenyl ring for the mono-substituted compounds of the same length. Azobenzenes with alkyl tails longer than three carbon atoms do not fit inside the capsule.[32,33]

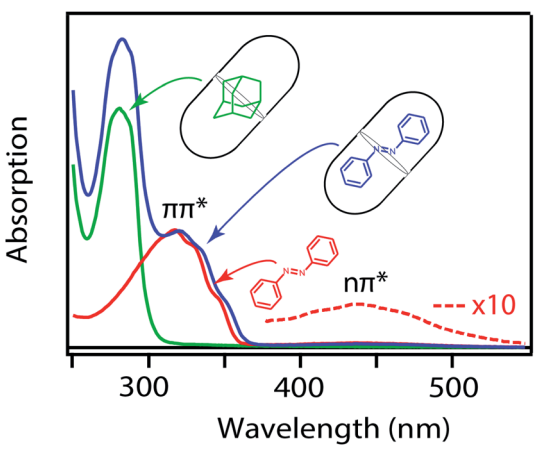

Fig. 2 Ground-state absorption spectra of *t*-Az in cyclohexane (red), *t*-Az@OA_2 (blue), and adamantane@OA_2 (green). Adamantane is transparent in this wavelength range.

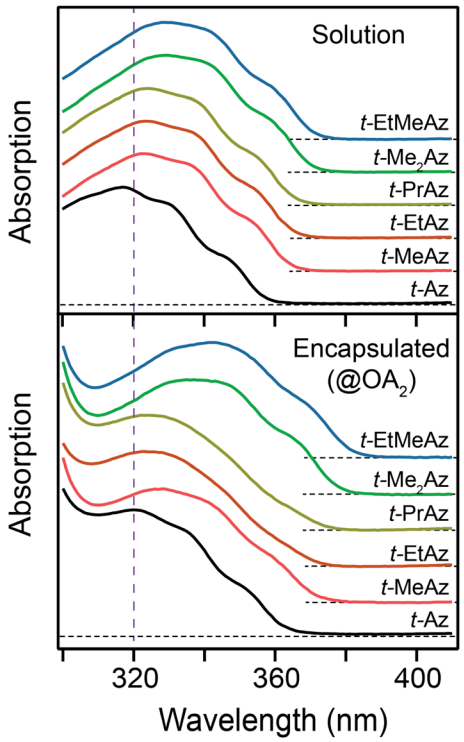

Fig. 3 Ground-state ππ* absorption band for the series of *t*-Az derivatives in cyclohexane (top panel) and in the OA_2 capsule (bottom panel). Vertical dashed line indicates the excitation wavelength of 320 nm.

Table 1 Photoisomerization quantum yields $\Phi_{t\rightarrow c}$ for ππ* excitation at 320 nm[a]

	$\Phi_{t\rightarrow c}$(solution)	$\Phi_{t\rightarrow c}$(capsule)
t-Az	0.11(4)	0.05(3)
t-MeAz	0.10(4)	0.10(4)
t-EtAz	0.15(4)	0.12(4)
t-PrAz	0.12(4)	0.17(4)
t-Me_2Az	0.13(4)	0.05(3)
t-EtMeAz	0.13(4)	0.03(2)

[a] Estimated 2σ uncertainties for the absolute quantum yields in parentheses. The relative uncertainties are smaller due to back-to-back measurements under identical conditions.

Open Access Article. Published on 24 August 2020. Downloaded on 4/19/2026 12:43:29 PM.
This article is licensed under a Creative Commons Attribution-NonCommercial 3.0 Unported Licence.

We report the *trans* → *cis* photoisomerization quantum yields ($\Phi_{t\rightarrow c}$) for ππ* excitation of all six compounds in Table 1. The estimated 2σ uncertainties in the table are for the absolute quantum yields, but the relative uncertainty between the measurements is much smaller because we made back-to-back measurements using identical conditions. The quantum yields are similar for all of the compounds in solution, ranging from 0.10 to 0.15, but vary considerably for the encapsulated compounds. The quantum yield increases systematically with chain length for the encapsulated mono-substituted compounds, from 0.05 for unsubstituted *t*-Az@OA_2 to 0.17 for the molecule with the longest alkyl chain, *t*-PrAz@OA_2. Notably, the value for *t*-PrAz@OA_2 is even larger than the quantum yield for the same molecule in solution. In contrast with the mono-substituted compounds of similar total length, the quantum yields for the encapsulated dialkyl-substituted azobenzenes *t*-Me_2Az@OA_2 and *t*-EtMeAz@OA_2 are only 0.05 and 0.03, respectively, which are much lower than the corresponding value of 0.13 in solution.

3.2 Transient absorption spectroscopy

The top panel of Fig. 4 shows the evolution of the transient absorption (TA) spectrum following nπ* excitation of unsubstituted *t*-Az in cyclohexane. The transient spectrum has a strong excited-state absorption (ESA) band centered near 395 nm and a weaker band near 540 nm. As reported previously,[18,21] the stronger absorption band shifts and narrows slightly due to vibrational relaxation within the first few hundred fs, then both bands decay simultaneously to the baseline within a few ps as excited molecules return to the ground state. A weak absorption feature below 375 nm persists for up to ~20 ps due to broadening and red-shifting of the ground-state ππ* absorption band for the vibrationally excited *trans* isomer.[45] Consistent with the low quantum yield for *trans* → *cis* isomerization of azobenzene (Table 1),[46] the TA signal essentially returns to the baseline at longer delay times.

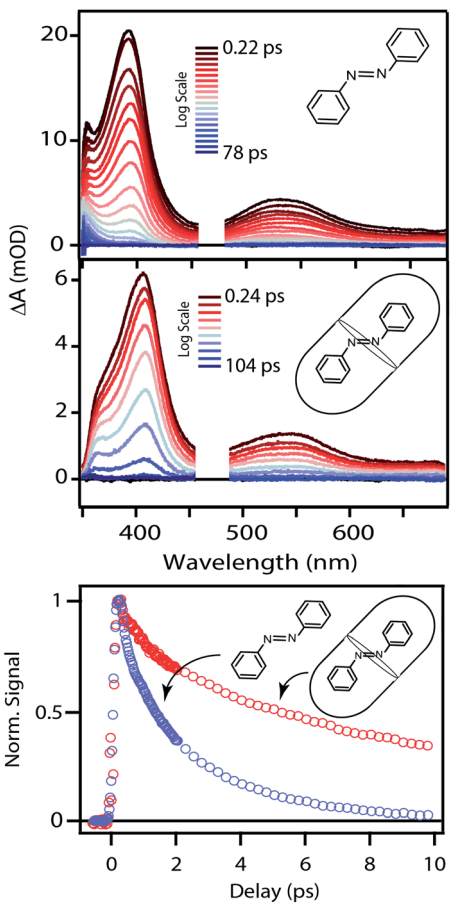

Fig. 4 Evolution of the TA spectra following nπ* excitation at 470 nm for *t*-Az in cyclohexane and Az@OA_2 at PSS. The bottom panel compares the decay at the maximum of the excited-state absorption bands.

The middle panel of Fig. 4 shows the evolution of the TA spectrum for nπ* excitation of Az@OA_2 at photo-stationary state (PSS). We use PSS in this case in order to avoid variation of the background signal from direct excitation of *c*-Az@OA_2 at 470 nm. Unlike the experiments in solution, the accumulation of *c*-Az@OA_2 is difficult to avoid for nπ* excitation in the small-volume sample due to the very slow thermal *cis* → *trans* recovery of the encapsulated molecules.[47] Even a small population of *c*-Az@OA_2 contributes to the TA signal because the molar absorbance of the *cis* isomer is nearly three times larger than *trans* at this excitation wavelength. Although the measurement at PSS contains contributions from both isomers, the relative concentration remains constant throughout the duration of the measurement, and therefore simplifies the analysis. Based on the ground-state absorption spectra of the two isomers (Fig. S1†), we estimate that ~23% of encapsulated molecules are in the *cis* geometry at PSS, giving an initial excited-state population consisting of ~40% *cis* and ~60% *trans*.

Despite the simultaneous excitation of both *c*-Az@OA_2 and *t*-Az@OA_2, the TA spectrum for the encapsulated sample at PSS is very similar to the spectrum of *t*-Az in solution, suggesting that the *trans* isomer provides the dominant contribution to the transient signal. Consistent with this observation, our global fits to the TA data (described below) reveal only a weak contribution from the excited state of *c*-Az@OA_2. However, the ESA band shifts to slightly longer wavelength and decays much slower in the capsule than in solution, as illustrated in the bottom panel of Fig. 4. The ~10 nm shift of the ESA band is similar to the shift of the ground-state ππ* absorption band in Fig. 2. The longer excited-state lifetime in the capsule prevents accumulation of vibrationally excited molecules in the ground state, which was responsible for the positive absorption feature below ~375 nm in cyclohexane. At the same time, the shift of the ground-state absorption band results in a transient ground-state bleach, and therefore appears as a steep reduction of the TA signal below ~360 nm that we do not observe in cyclohexane for the same range of probe wavelengths.

The TA spectra following ππ* excitation of *t*-Az and *t*-Az@OA_2 are shown in Fig. 5, where we divide the evolution of the spectra into separate panels to better represent the rapid relaxation from S_2 to S_1 within the first ~200 fs, and the subsequent relaxation from S_1 to S_0 on a longer time scale.[34] Unlike the nπ* experiments above, PSS is unnecessary in the case of UV excitation, because the significantly weaker

 This journal is © The Royal Society of Chemistry 2020

Open Access Article. Published on 24 August 2020. Downloaded on 4/19/2026 12:43:29 PM.
This article is licensed under a Creative Commons Attribution-NonCommercial 3.0 Unported Licence.

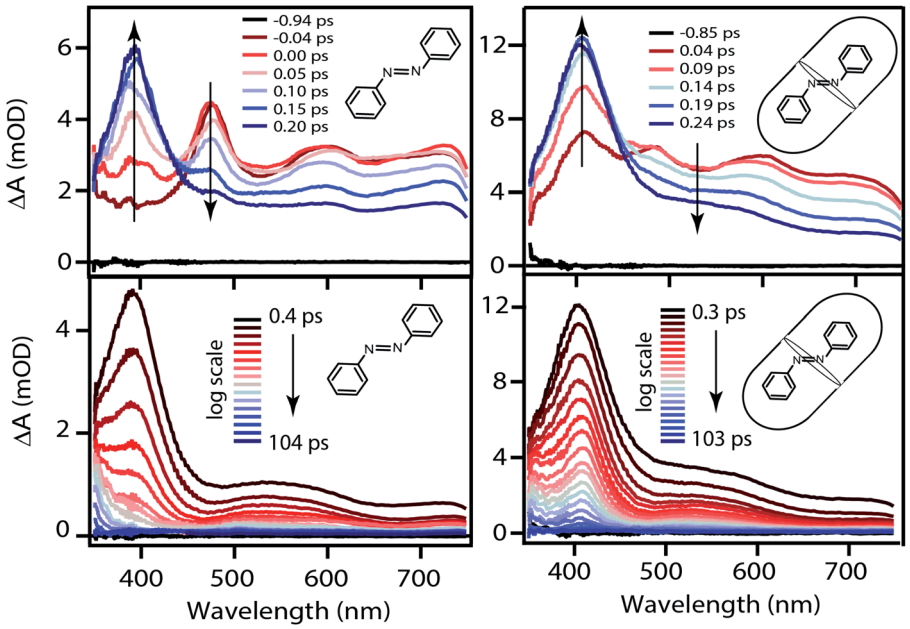

Fig. 5 Evolution of the TA spectra following ππ* excitation at 320 nm of *t*-Az in cyclohexane (left) and *t*-Az@OA_2 (right). The upper panels show only the first few hundred fs, the lower panels show the evolution up to ~100 ps.

absorption of the *cis* isomer at 320 nm results in a negligible contribution to the transient signal from direct excitation of that isomer. The lower isomerization yield for UV excitation also reduces the amount of *cis* isomer that forms. Comparing the static absorption spectra before and after each TA measurement confirms that there is minimal accumulation of *cis* isomer over the duration of the experiment for ππ* excitation.

The initial ESA spectrum following ππ* excitation has several broad features, including a prominent absorption band near 485 nm and weaker bands near 600 and 710 nm.[45,48] This spectrum is similar in both samples, except for additional broadening of the individual ESA bands for the encapsulated compound. In both cases, the S_2 absorption decays within ~100 fs and is replaced by a spectrum that is very similar to the S_1 spectrum that we observe following direct nπ* excitation at 470 nm. An isobestic point near ~450 nm confirms direct relaxation from S_2 to S_1 in both environments. The slight broadening of the S_1 spectra compared with Fig. 4 probably reflects excess vibrational energy following internal conversion from S_2.

3.3 Kinetic models

Global fits to the TA spectra reveal more detailed information about the excited-state dynamics. We use a combination of singular value decomposition (SVD)[49] and fits to the TA data with a sum of exponentials (*e.g.* Fig. S3†) to determine the smallest number of time constants that are necessary to accurately reproduce the evolution of each spectrum. We then use target analysis to apply more restrictive kinetic models in the fits to the data.[50] Target analysis gives species-associated spectra (SAS) that represent individual states in the kinetic model, where the time evolution of the spectra are restricted by the specified pathways between states. All of the fits include a convolution of the kinetics with a Gaussian instrument response function (100 fs fwhm) to account for the time-resolution of our measurement. We allow all of the time constants and amplitudes to vary in each of the fits, except where indicated otherwise.

3.3.1 nπ* excitation at 470 nm. The top panel of Fig. 6 shows the SAS and associated time constants for nπ* excitation of *t*-Az in solution. We model the kinetics in cyclohexane based on previous work showing a competition between relaxation pathways in the excited state.[28,34] The model begins with vibrationally excited S_1^* that relaxes through two competing channels, one that returns directly to the ground state in ~1 ps, and a second that undergoes vibrational relaxation in S_1 before returning to the ground state on a timescale of 2.4 ps. This branching in the excited state represents a bifurcation between one pathway that directly accesses a conical intersection with the ground state and a second pathway that relaxes to a minimum-energy structure in the excited state before crossing a barrier to reach either the same or a different conical intersection.[20] Both channels lead to the vibrationally hot ground state, S_0^*, which then dissipates energy to the solvent to reach the equilibrated S_0 on a timescale of 13.0 ps. Importantly, the SAS from the fits are consistent with the kinetic model, including a slight shift and narrowing of the primary ESA band from S_1^* to S_1, and a tail below ~375 nm due to broadening of the ππ* absorption band for S_0^* compared with S_0.[45] The model does not distinguish between *cis* and *trans* isomers in the relaxed ground state, because the weak contribution from S_0^* is not sufficient to determine the branching ratio directly from the TA measurements.

The bottom panel of Fig. 6 shows the SAS that we obtain for nπ* excitation of the mixed isomers of Az@OA_2 at PSS. We use

Open Access Article. Published on 24 August 2020. Downloaded on 4/19/2026 12:43:29 PM.
This article is licensed under a Creative Commons Attribution-NonCommercial 3.0 Unported Licence.

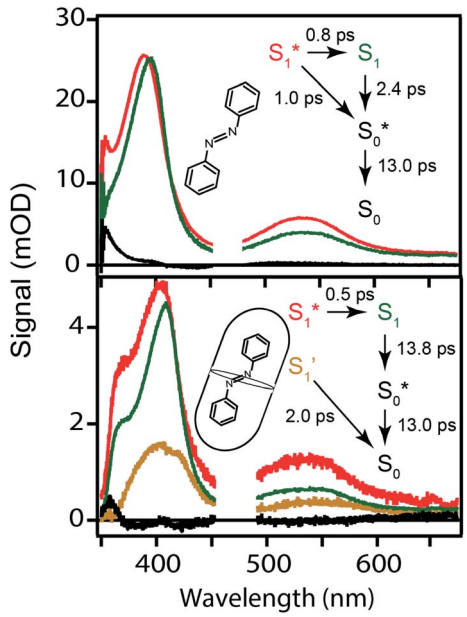

Fig. 6 Species-associated spectra for nπ* excitation of *t*-Az in cyclohexane (top) and mixed *t*-Az@OA_2/*c*-Az@OA_2 at PSS (bottom). The kinetic models and lifetimes from the global fits are shown in the insets. See text for details.

a kinetic model with parallel contributions for the *cis* and *trans* isomers, as shown in the inset. The model for relaxation of *t*-Az@OA_2 is similar to the model in solution, except that we do not observe a rapid decay of the total TA signal strength within the first ps for the encapsulated molecule, and therefore do not include a direct relaxation channel from S_1^* to S_0^* in the capsule. Instead, the ESA band decays on a single timescale of 13.8 ps, compared with the 2.4 ps lifetime in solution. Despite the very different excited-state lifetimes, the SAS for *t*-Az@OA_2 are remarkably similar to the spectra in cyclohexane. It is not necessary to include ground-state vibrational cooling ($S_0^* \rightarrow S_0$) in order to accurately reproduce the TA spectrum for the encapsulated sample, but we find that adding this component with a fixed lifetime of 13.0 ps recovers a weak signature below 375 nm that is similar to the vibrationally hot S_0^* in solution. The spectrum for S_0^* is much noisier in the capsule because the hot ground state cools on the same timescale as the electronic relaxation from S_1, and therefore prevents accumulation of highly vibrationally excited molecules.

The global fits reveal an additional feature in the evolution of the TA spectrum of the mixed encapsulated isomers that decays on a time scale of 2.0 ps. We confidently assign this feature as the excited state of *c*-Az@OA_2, because the SAS (gold spectrum in Fig. 6) has absorption bands near 400 and 550 nm that closely resemble the ESA spectrum for nπ* excitation of *c*-Az in solution.[21] The previously reported spectrum for *c*-Az has broader and weaker absorption bands than the excited-state spectrum of the *trans* isomer, just like we observe here. Although the 2.0 ps lifetime that we observe for *c*-Az@OA_2 is significantly longer than the ~100 fs lifetime previously reported for *c*-Az in solution,[21,45,51] this difference mirrors the order-of-magnitude longer lifetime of the *trans* isomer in the capsule compared with solution.

3.3.2 ππ* excitation at 320 nm. We analyze the evolution of the TA spectrum following ππ* excitation of *t*-Az in cyclohexane using a similar kinetic model as nπ* excitation, except for the addition of an initial relaxation step from S_2 to S_1^*. In order to improve the quality of the fits we fix the $S_2 \rightarrow S_1^*$ internal conversion time at 50 fs based on measurements with higher time resolution by Nenov, *et al.*[28] The top panel of Fig. 7 shows the SAS. The spectra for S_1^*, S_1, and S_0^* are all very similar to the spectra from nπ* excitation, with some additional broadening of S_1^* that is probably a signature of excess vibrational energy following internal conversion from S_2.[42] The spectrum for S_2 is distinct from the other states, and includes a negative stimulated emission band near 400 nm that closely matches an $S_2 \rightarrow S_0$ fluorescence band that was previously reported following ππ* excitation of *t*-Az.[22,52]

Importantly, the kinetic model for ππ* excitation of *t*-Az@OA_2 requires an additional component compared with *t*-Az in cyclohexane. The additional lifetime is evident from both SVD and the global fits to the data using a sum of exponentials, each of which suggests that a total of at least five time constants are necessary to accurately reproduce the evolution of the experimental TA spectrum for the encapsulated sample. Thus, in addition to the initially excited S_2, we include an extra feature (S_1') for the encapsulated molecule. The kinetic model that gives the best agreement with experiment is shown in the bottom panel of Fig. 7, along with the resulting SAS from target analysis. We tested several different kinetic models, but only this model, which includes three distinct channels for the relaxation of S_1^*,

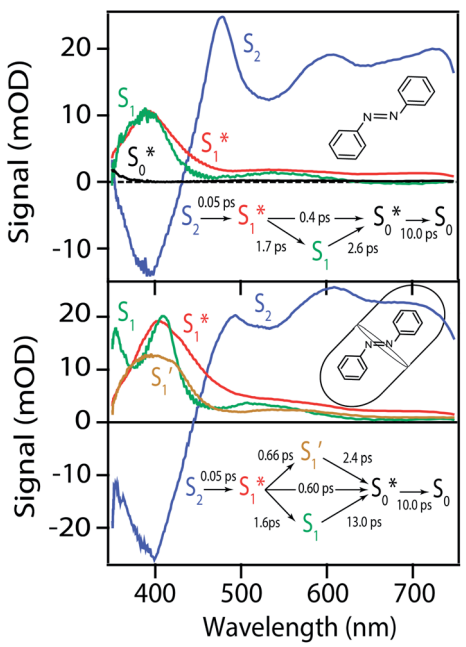

Fig. 7 Species associated spectra for ππ* excitation of azobenzene in cyclohexane (top) and the OA_2 capsule (bottom). The spectra are from global fits to the transient absorption spectra using the kinetic models shown in the insets. See text for details.

This journal is © The Royal Society of Chemistry 2020

Open Access Article. Published on 24 August 2020. Downloaded on 4/19/2026 12:43:29 PM.
This article is licensed under a Creative Commons Attribution-NonCommercial 3.0 Unported Licence.

gives a good fit to the data and also is consistent with the results from above. We exclude other kinetic models based on poor fits to the data or unreasonable results, such as artificially short lifetimes (*i.e.* <50 fs) for species other than S_2, or SAS with negative spectral features above 500 nm. As before, we convoluted the fits with a 100 fs instrument-response function, and used a fixed lifetime of 50 fs for the relaxation of S_2.

The SAS for S_2 and S_1^* of *t*-Az@OA_2 are similar to the spectra in solution, and decay on roughly the same two time scales (50 fs and ~300 fs, respectively) in both environments. However, a key result from the model for ππ* excitation of *t*-Az@OA_2 is the presence of two distinct excited-state species (S_1 and S_1') with lifetimes of 13 and 2.4 ps, respectively. We assign the species with a lifetime of 13 ps as the relaxed S_1 state of *t*-Az@OA_2, based on the similar spectrum and lifetime that we observe following nπ* excitation of the encapsulated molecule. We assign the other feature, S_1', as the relaxed excited state of the *cis* isomer, even though we excite only the *trans* isomer of the encapsulated compound at 320 nm. Importantly, both the spectrum and the 2.4 ps lifetime of S_1' closely match the spectrum and lifetime that we observe following direct nπ* excitation of *c*-Az@OA_2 at 470 nm. Formation of the *cis* excited state after ππ* excitation of *t*-Az@OA_2 implies adiabatic isomerization in S_1, which we observe only at the higher excitation energy and in the confined environment of the capsule.

3.3.3 Alkyl-substituted azobenzenes. The TA spectra for ππ* excitation of the five alkyl-substituted azobenzenes in solution and in the capsule are shown in Fig. S5 and S6 of the ESI.† In cyclohexane, the spectra and decay times for all five molecules are essentially the same as unsubstituted *t*-Az, therefore we model the evolution of the TA spectra using the same kinetic model in each case. The global fits give similar lifetimes and SAS for all six compounds in solution, regardless of alkyl substitution. In contrast, the decay times for the encapsulated compounds depend on both the number and length of alkyl substituents. We also find that the kinetic models require some variation with the structure of the molecule in order to give reasonable fits for the encapsulated samples. The main difference is whether or not we include a channel for direct relaxation from S_1^* to the ground state. For unsubstituted *t*-Az@OA_2 and the mono-alkyl substituted derivatives, we observe rapid decay of the ESA that requires the direct $S_1^* \rightarrow S_0^*$ relaxation channel. The same model gives a poor fit to the data for the di-substituted azobenzenes, Me_2Az@OA_2 and EtMeAz@OA_2, where the TA spectra do not rapidly decrease in intensity after the initial electronic relaxation to S_1^*. Instead, we remove the direct $S_1^* \rightarrow S_0^*$ relaxation channel from the model for these two compounds. In all cases, we use a fixed lifetime of 10 ps for the S_0^* lifetime due to the insensitivity of the fit to this small-amplitude signal. The SAS for the full series of compounds are presented in the ESI† and the lifetimes of S_1 and S_1' are listed in Table 2.

Table 2 Excited-state lifetimes for ππ* excitation[a]

	Solution	Capsule	
	τ_{S_1} (ps)	τ_{S_1} (ps)	$\tau_{S_1'}$ (ps)
t-Az	2.6	13	2.4
t-MeAz	1.8	15	2.4
t-EtAz	2.3	21	3.8
t-PrAz	2.5	26	5.6
t-Me_2Az	2.4	35	3.3
t-EtMeAz	2.6	55	3.5

[a] From global fits using the kinetic models described in the text. For encapsulated molecules, the model includes two distinct excited-state species, S_1 and S_1'.

A comparison of the lifetimes of the encapsulated molecules with those in solution is informative. While the S_1 lifetimes are essentially the same for all of the compounds in solution (~2.5 ps), the lifetimes are significantly longer in the capsule, ranging from 13 ps for unsubstituted *t*-Az@OA_2 to 55 ps for *t*-EtMeAz@OA_2. The S_1' lifetimes in the capsule also depend on the length of the substituent, increasing from 2.4 to 5.6 ps for the mono-substituted compounds, with the di-substituted compounds having intermediate lifetimes.

Fig. 8 compares the SAS for the S_1 state of each compound in solution with the S_1 and S_1' spectra in OA_2. For the encapsulated compounds, we shade the S_1 spectra below 360 nm due to complications from overlapping spectral features in the target analysis. On one hand, the similar timescales for electronic relaxation of S_1 and vibrational cooling of S_0^* results in an artificial increase of the S_1 SAS below ~360 nm for *t*-Az@OA_2, *t*-MeAz@OA_2, and *t*-EtAz@OA_2. On the other hand, the red-shifted ground-state ππ* absorption bands for the two di-substituted compounds result in ground-state bleaching that is not accounted for in our model and therefore gives a steep decrease of the SAS below 360 nm. *t*-PrAz@OA_2 has a long enough S_1 lifetime and small enough shift of the ground-state absorption band that it is not susceptible to these issues, but the relative population of S_1 is much smaller in that case, giving a poorer signal-to-noise ratio for the SAS.

Neglecting the known discrepancies below 360 nm, Fig. 8 shows that the S_1 SAS are similar for all of the compounds, both in solution and in the capsule. However, the S_1' SAS are more variable across the series of encapsulated molecules. The main ESA band in the S_1' spectrum broadens and splits into two overlapping features with increasing length of the alkyl substituent. Notably, the spectra for S_1' of the di-substituted compounds have a different shape than the spectra for the mono-substituted compounds, including more pronounced splitting of the ESA band and higher intensity of the longer wavelength component near 440 nm. A weaker ESA band near 550 nm for Az@OA_2 and the encapsulated mono-substituted compounds also shifts ~50 nm to longer wavelength for the disubstituted compounds in the capsule.

4 Discussion

4.1 Isomerization mechanism

Our kinetic modeling and global fits reveal interesting details about the excited-state dynamics of *t*-Az in solution and in the capsule. The schematic potential energy diagrams in Fig. 9

Open Access Article. Published on 24 August 2020. Downloaded on 4/19/2026 12:43:29 PM.
This article is licensed under a Creative Commons Attribution-NonCommercial 3.0 Unported Licence.

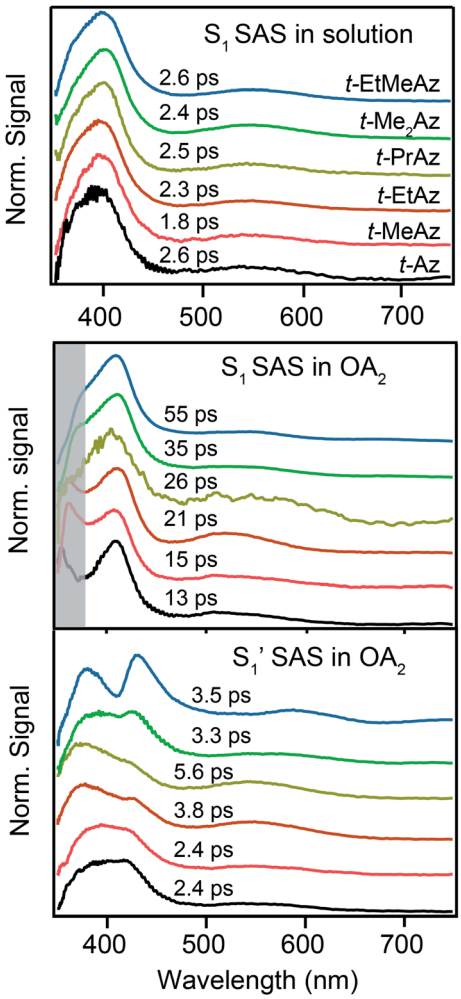

Fig. 8 The upper panel shows the SAS for S_1 in solution. The lower panels show the S_1 and S_1' SAS inside the OA_2 capsule. The shaded band indicates a region with known artifacts in the S_1 SAS of the encapsulated molecules.

illustrate the reaction pathways and lifetimes that we extract from the models for nπ* and ππ* excitation in each environment. An important difference between the models in Fig. 9 is the fast $S_1^* \rightarrow S_0^*$ electronic relaxation channel. We observe this prompt relaxation for both nπ* and ππ* excitation in solution, indicating that there is a direct pathway to access a conical intersection (or conical seam) with the ground state. However, not all molecules take this direct pathway, and some relax to a local minimum energy structure on the S_1 excited state. The excited-state lifetime of ~2.5 ps in solution represents the activated barrier crossing to escape the local minimum and access the region of the conical intersection. The topology of the conical intersection determines the branching between *trans* and *cis* isomers when molecules return to the ground electronic state.[26,53]

The direct pathway to the conical intersection has been identified as a likely explanation for the different quantum yields following nπ* and ππ* excitation.[28,34] The *trans* → *cis* isomerization yield for ππ* excitation to S_2 is lower than it is for direct nπ* excitation to S_1.[14] Although early reports attributed the different quantum yields to the different electronic character of the initially excited states, more recent explanations point to the role of excess vibrational energy following rapid internal conversion from S_2 to S_1^*.[17,54–56] Internal conversion from S_2 to S_1^* leaves the molecule with sufficient excess vibrational energy to access higher-energy regions of the S_1–S_0 conical seam, which preferentially leads back to the *trans* isomer in the ground state. Thus, the 'non-Kasha' behavior, *i.e.* the different reaction yields for excitation to S_2 and S_1, is a result of competition between rapid (few ps) isomerization and vibrational cooling in the excited state.

In contrast with the dynamics in solution, the direct $S_1^* \rightarrow S_0^*$ relaxation pathway is absent for nπ* excitation in the capsule, where steric restrictions may inhibit the motions required to access the conical seam. Steric restriction is consistent with the larger barrier to escape the S_1 local minimum and therefore the longer excited-state lifetime of 13.8 ps in the capsule compared with only 2.4 ps in solution. However, the fast electronic relaxation pathway becomes accessible again in the capsule for higher-energy excitation into the ππ* band. Excitation of the ππ* band provides enough energy to overcome the barrier (including steric restrictions) after internal conversion from S_2.

Our results are consistent with the proposed reaction mechanism of Nenov *et al.*,[28] who showed that the minimum-energy reaction path for freely solvated *t*-Az involves inversion-assisted rotation on S_1. This reaction path begins with in-plane bending of a phenyl ring along the inversion coordinate, then includes some out-of-plane rotation to access a conical intersection with the ground state. The inversion-assisted rotation mechanism results from mixing of the nπ* and ππ* states along the reaction coordinate.[27] In the capsule, the deeper local minimum on the S_1 potential inhibits the motion to access the region of the conical intersection, possibly due to distortion of the molecule into a nonplanar geometry that inhibits the proposed initial motion along the in-plane inversion coordinate. For ππ* excitation, rapid internal conversion from S_2 provides sufficient excess energy for the molecule to deviate from the minimum-energy path and overcome the larger barrier at nonplanar geometries. The ~50 fs lifetime of S_2 suggests that the motion toward the conical seam probably occurs in the vibrationally excited S_1^*, rather than S_2. The timescales for the initial relaxation from S_2 to S_1 and the vibrational and structural relaxation on S_1 are essentially the same in both environments, indicating that the early relaxation processes are largely insensitive to confinement.[57]

Another key result from our measurements is the observation of the second excited-state species, S_1', after ππ* excitation in the capsule. Although we excite *c*-Az@OA_2 directly in the nπ* excitation experiments at PSS, the measurements for ππ* excitation use a pure solution of *t*-Az@OA_2. Nevertheless, we observe the same S_1' absorption feature in both cases. The two distinct excited-state features indicate the presence of both *trans* and *cis* excited-state structures following ππ* excitation of *t*-Az@OA_2. This implies an excited-state isomerization pathway, probably on the S_1 potential energy surface. Adiabatic isomerization to populate the *trans* excited state after excitation of the

 This journal is © The Royal Society of Chemistry 2020

Open Access Article. Published on 24 August 2020. Downloaded on 4/19/2026 12:43:29 PM.
This article is licensed under a Creative Commons Attribution-NonCommercial 3.0 Unported Licence.

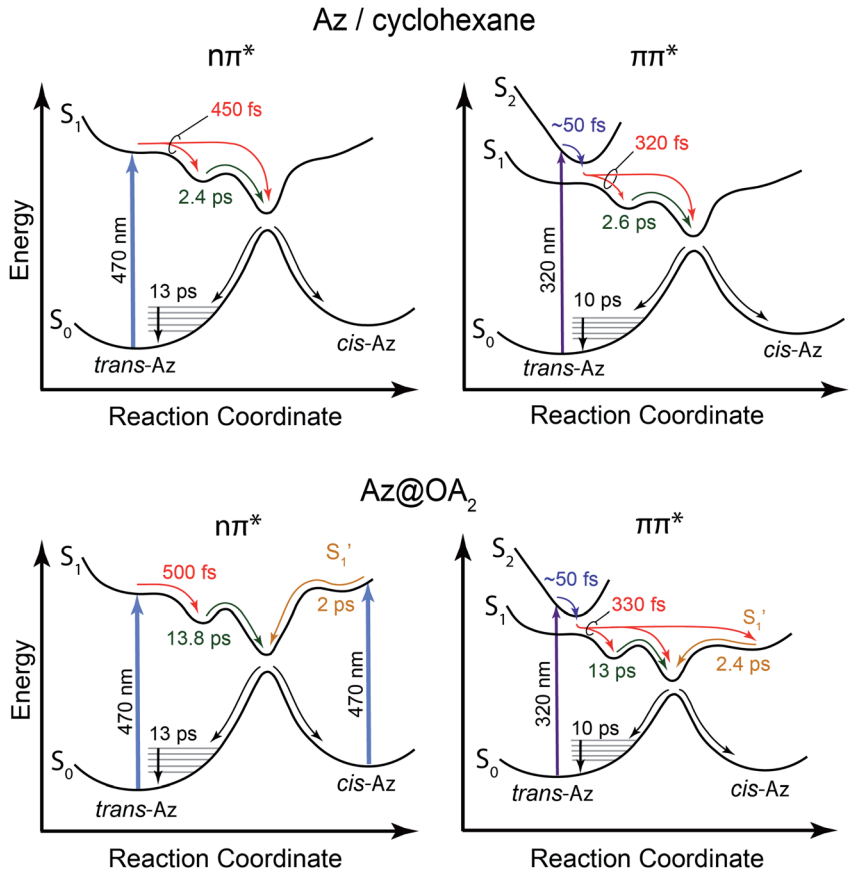

Fig. 9 Schematic diagram of the potential energy curves for Az in cyclohexane (top) and Az@OA_2 (bottom). The left side shows the reaction pathway for nπ* excitation, and the right side shows ππ* excitation.

cis isomer has been observed,[45] but the encapsulated azobenzenes in OA_2 are the first example to our knowledge showing the reverse process of *trans* → *cis* excited-state isomerization.

Our results support an emerging picture that molecules may explore a wide range of structures in the excited state even though the reaction dynamics are largely determined by the minimum-energy path.[58,59] In other words, the excited-state wave packet may sample both *cis* and *trans* regions of the potential, even in solution, but we observe the *cis* isomer only in the capsule due to "trapping" of that structure in the restricted environment of the capsule. Branching between the three channels (*i.e.*, the direct pathway to the ground state, and relaxation to the *trans* and *cis* local minima) depends on the relative time scales for vibrational cooling and to explore energetically accessible regions of the excited-state potential energy surface. Vibrational relaxation essentially quenches the excited-state dynamics within a few hundred fs, trapping the molecules in any accessible local minima. We observe the encapsulated *cis* isomer because of the deeper well in the confined environment, which is evident from the significantly longer lifetime of 2 ps for *c*-Az@OA_2 compared with the sub-100 fs lifetime of *c*-Az in solution.[45] This picture suggests that excitation of the ππ* band not only provides enough energy to overcome the barrier to access the S_1–S_0 conical intersection directly, but also to reach the *cis* geometry of the excited state.

4.2 Crowding effects

The variation of the excited-state lifetimes and spectra across the series of encapsulated alkyl-substituted azobenzenes reveals additional changes in the excited-state dynamics due to confinement. In solution, the lifetimes and spectra are essentially independent of alkyl substitution, therefore the differences among the encapsulated compounds are largely due to steric restrictions of the capsule. Increasing the alkyl-chain length probes the role of crowding on the reaction dynamics because longer molecules have less space to rearrange. The similar lifetimes in solution are due to the substituents having little influence on the π-conjugation, and being located at the *para* position of the phenyl rings, where they do not inhibit the isomerization.

For *t*-Az@OA_2 and the encapsulated mono-substituted compounds, the excited-state lifetime increases with chain length, suggesting a deeper local minimum on S_1 with increasing size. This is consistent with an increasingly distorted excited-state geometry in the capsule that inhibits the initial in-plane motion along the inversion-assisted rotational reaction coordinate. More distortion due to increased crowding results in a larger barrier to reach the region of the conical intersection, and therefore the longer excited-state lifetimes compared with solution. The minimum-energy pathway in solution starts from

Open Access Article. Published on 24 August 2020. Downloaded on 4/19/2026 12:43:29 PM.
This article is licensed under a Creative Commons Attribution-NonCommercial 3.0 Unported Licence.

a planar structure on the S_1 surface, for which the barrier height is smallest.[20] At the same time that the S_1 lifetime increases, we also observe a significant distortion of the S_1' spectrum with increasing chain length. The splitting of the S_1' SAS into two bands suggests that the electronic structure of the S_1' state changes across the series of encapsulated molecules. The progressive change in the S_1' SAS for the mono-substituted compounds probably represents increasing distortion as the chain length increases, a trend that is also evident in the ground-state where the ππ* absorption bands indicate a distorted, nonplanar geometry of the longest mono-substituted compounds, *t*-EtAz@OA_2 and *t*-PrAz@OA_2.

The dynamics are even more sensitive to encapsulation for the di-substituted compounds, which prefer to remain in the *trans* structure due to stable packing of the alkyl tails in the ends of the capsule. For example, the absence of a fast $S_1^* \rightarrow S_0^*$ relaxation channel for the disubstituted compounds indicates that encapsulation prevents these molecules from easily accessing the region of the conical seam, even after excitation to the higher-energy ππ* state. Favorable packing of the alkyl tails into the two ends of the OA_2 capsule favors the extended *trans* geometry, and possibly stabilizes an excited-state structure that then inhibits the isomerization. The favorable packing of the *trans* isomer of the disubstituted compounds is also reflected in the very low isomerization quantum yields for the two encapsulated molecules compared with solution and with the other encapsulated compounds (Table 1).

The interaction of the alkyl tails with the capsule provides an explanation for the variation of the S_1' SAS across the series of encapsulated compounds. An unsubstituted phenyl ring does not fit into the ends of the capsule as well as the smaller alkyl tails, therefore crowding favors the more compact structure of the *cis* isomer to compensate the lengthening of the molecule with increasing alkyl chain length. The unsubstituted and mono-substituted compounds therefore increasingly favor the *cis* structure as the length of the tail increases, resulting in the higher quantum yields and stronger perturbation of the SAS as crowding becomes more severe.[35] In contrast, the di-substituted compounds always favor the *trans* structure, and even the S_1' state probably retains a more distorted *trans*-like structure for these molecules in the capsule. Excited-state simulations for the encapsulated compounds would be helpful to elucidate the structures, but the very low quantum yield for disubstituted compounds clearly shows the impact of alkyl tails in changing the reaction path inside the OA_2 capsule.

Finally, we point out that confinement probably also affects the topology at the conical seam directly, leading to a lower quantum yield for ππ* excitation in the capsule (5%) compared with solution (11%) even for unsubstituted *t*-Az. The impact becomes greater with increased crowding, and it is interesting to note that the isomerization quantum yield actually increases in the capsule compared with solution for the longest mono-substituted compound. This result is not entirely surprising considering the change in relative stability of the *trans* and *cis* isomers with increasing chain length,[35] but nevertheless highlights the sensitivity of the excited-state dynamics and reaction pathways to confinement.

5 Conclusion

The ultrafast spectroscopy for a series of encapsulated alkyl-substituted azobenzene derivatives provides insight into the fundamental photoisomerization reaction following nπ* and ππ* excitation. In comparison with the azobenzene derivatives in solution we observe the encapsulated azobenzene molecules to have increasing excited-state lifetimes with increasing molecular length when relaxing from the S_1 state due to the increasing sterical hindrance for phenyl rotational motion within the capsule. The confined environment opens up an additional relaxation pathway leading to a S_1' species, which for the mono-substituted derivatives resembles the formation of the *cis* excited-state isomer. Restricting the excited-state dynamics with di-substitution at the 4 and 4′ positions of the azobenzene molecule greatly impedes the inversion mechanism, which results in significantly lower *trans* → *cis* quantum yields and an S_1' species that has a highly out-of-plane distorted geometry. The fundamentally different behavior observed in the confined environment demonstrates the importance of understanding the unique mechanisms for the isomerization of azobenzene, including the non-Kasha behavior that results in different quantum yields for nπ* and ππ* excitation.

Conflicts of interest

There are no conflicts to declare.

Acknowledgements

This material is based upon work supported by the National Science Foundation under grants CHE-1151555 (C. G. E.) and CHE-1807729 (V. R.). C. J. O. also acknowledges support by the US Department of Energy, Office of Basic Energy Sciences, Division of Chemical Sciences, Geosciences, and Biosciences through Argonne National Laboratory under Contract No. DE-AC02-06CH11357.

Notes and references

1 C. Dugave and L. Demange, *Chem. Rev.*, 2003, **103**, 2475–2532.
2 A. A. Beharry and G. A. Woolley, *Chem. Soc. Rev.*, 2011, **40**, 4422–4437.
3 O. P. Ernst, D. T. Lodowski, M. Elstner, P. Hegemann, L. S. Brown and H. Kandori, *Chem. Rev.*, 2014, **114**, 126–163.
4 M. Vengris, M. A. van der Horst, G. Zgrablić, I. H. M. van Stokkum, S. Haacke, M. Chergui, K. J. Hellingwerf, R. van Grondelle and D. S. Larsen, *Biophys. J.*, 2004, **87**, 1848–1857.
5 P. Kukura, D. W. McCamant, S. Yoon, D. B. Wandschneider and R. A. Mathies, *Science*, 2005, **310**, 1006.
6 D. Polli, P. Altoè, O. Weingart, K. M. Spillane, C. Manzoni, D. Brida, G. Tomasello, G. Orlandi, P. Kukura, R. A. Mathies, M. Garavelli and G. Cerullo, *Nature*, 2010, **467**, 440.
7 S. Gozem, H. L. Luk, I. Schapiro and M. Olivucci, *Chem. Rev.*, 2017, **117**, 13502–13565.

 This journal is © The Royal Society of Chemistry 2020

Open Access Article. Published on 24 August 2020. Downloaded on 4/19/2026 12:43:29 PM.
This article is licensed under a Creative Commons Attribution-NonCommercial 3.0 Unported Licence.

8 Y. Norikane and N. Tamaoki, *Org. Lett.*, 2004, **6**, 2595–2598.
9 A. Sobolewska, S. Bartkiewicz, A. Miniewicz and E. Schab-Balcerzak, *J. Phys. Chem. B*, 2010, **114**, 9751–9760.
10 E. A. Dolgopolova, T. M. Moore, O. A. Ejegbavwo, P. J. Pellechia, M. D. Smith and N. B. Shustova, *Chem. Commun.*, 2017, **53**, 7361–7364.
11 H. Rau, *Angew. Chem., Int. Ed.*, 1973, **12**, 224–235.
12 H. Rau, in *Photochromism: Molecules and Systems*, ed. H. Durr and H. Bouas-Laurent, Elsevier, 1990, ch. 4, pp. 165–192.
13 G. Kumar and D. Neckers, *Chem. Rev.*, 1989, **89**, 1915–1925.
14 H. M. D. Bandara and S. C. Burdette, *Chem. Soc. Rev.*, 2012, **41**, 1809–1825.
15 Y. Kim, J. A. Phillips, H. Liu, H. Kang and W. Tan, *Proc. Natl. Acad. Sci. U. S. A.*, 2009, **106**, 6489–6494.
16 J. Wang, H.-B. Liu and C.-S. Ha, *Tetrahedron*, 2009, **65**, 9686–9689.
17 E. Wei-Guang Diau, *J. Phys. Chem. A*, 2004, **108**, 950–956.
18 I. K. Lednev, T.-Q. Ye, R. E. Hester and J. N. Moore, *J. Phys. Chem.*, 1996, **100**, 13338–13341.
19 C. M. Stuart, R. R. Frontiera and R. A. Mathies, *J. Phys. Chem. A*, 2007, **111**, 12072–12080.
20 T. Fujino and T. Tahara, *J. Phys. Chem. A*, 2000, **104**, 4203–4210.
21 H. Satzger, C. Root and M. Braun, *J. Phys. Chem. A*, 2004, **108**, 6265–6271.
22 T. Fujino, S. Y. Arzhantsev and T. Tahara, *J. Phys. Chem. A*, 2001, **105**, 8123–8129.
23 C.-W. Chang, Y.-C. Lu, T.-T. Wang and E. W.-G. Diau, *J. Am. Chem. Soc.*, 2004, **126**, 10109–10118.
24 H. Rau and E. Luddecke, *J. Am. Chem. Soc.*, 1982, **104**, 1616–1620.
25 H. Rau, *J. Photochem.*, 1984, **26**, 221–225.
26 L. Blancafort, *ChemPhysChem*, 2014, **15**, 3166–3181.
27 Y. Hirose, H. Yui and T. Sawada, *J. Phys. Chem. A*, 2002, **106**, 3067–3071.
28 A. Nenov, R. Borrego-Varillas, A. Oriana, L. Ganzer, F. Segatta, I. Conti, J. Segarra-Marti, J. Omachi, M. Dapor, S. Taioli, C. Manzoni, S. Mukamel, G. Cerullo and M. Garavelli, *J. Phys. Chem. Lett.*, 2018, 1534–1541.
29 N. Turro, V. Ramamurthy, W. Cherry and W. Farneth, *Chem. Rev.*, 1978, **78**, 125–145.
30 T. Itoh, *Chem. Rev.*, 2012, **112**, 4541–4568.
31 A. P. Demchenko, V. I. Tomin and P.-T. Chou, *Chem. Rev.*, 2017, **117**, 13353–13381.
32 S. R. Samanta, A. Parthasarathy and V. Ramamurthy, *Photochem. Photobiol. Sci.*, 2012, **11**, 1652–1660.
33 A. Parthasarathy and V. Ramamurthy, *Photochem. Photobiol. Sci.*, 2011, **10**, 1455–1462.
34 C. J. Otolski, A. M. Raj, V. Ramamurthy and C. G. Elles, *J. Phys. Chem. Lett.*, 2019, **10**, 121–127.
35 C. J. Otolski, A. M. Raj, G. Sharma, R. Prabhakar, V. Ramamurthy and C. G. Elles, *J. Phys. Chem. A*, 2019, **123**, 5061–5071.
36 A. Parthasarathy, L. S. Kaanumalle and V. Ramamurthy, *Org. Lett.*, 2007, **9**, 5059–5062.
37 C. L. D. Gibb and B. C. Gibb, *J. Am. Chem. Soc.*, 2004, **126**, 11408–11409.
38 V. Ramamurthy and A. Parthasarathy, *Isr. J. Chem.*, 2011, **51**, 817–829.
39 V. Ramamurthy, *Acc. Chem. Res.*, 2015, **48**, 2904–2917.
40 A. Mohan Raj and V. Ramamurthy, *Org. Lett.*, 2017, **19**, 6116–6119.
41 I. L. Zheldakov, J. M. Wasylenko and C. G. Elles, *Phys. Chem. Chem. Phys.*, 2012, **14**, 6211–6218.
42 A. L. Houk, I. L. Zheldakov, T. A. Tommey and C. G. Elles, *J. Phys. Chem. B*, 2015, **119**, 9335–9344.
43 C. L. Ward and C. G. Elles, *J. Phys. Chem. A*, 2014, **118**, 10011–10019.
44 L. Landt, M. Staiger, D. Wolter, K. Klünder, P. Zimmermann, T. M. Willey, T. v. Buuren, D. Brehmer, P. R. Schreiner, B. A. Tkachenko, A. A. Fokin, T. Möller and C. Bostedt, *J. Chem. Phys.*, 2010, **132**, 024710.
45 M. Quick, A. L. Dobryakov, M. Gerecke, C. Richter, F. Berndt, I. N. Ioffe, A. A. Granovsky, R. Mahrwald, N. P. Ernsting and S. A. Kovalenko, *J. Phys. Chem. B*, 2014, **118**, 8756–8771.
46 P. Bortolus and S. Monti, *J. Phys. Chem.*, 1979, **83**, 648–652.
47 M. Moreno, R. Gelabert and J. M. Lluch, *ChemPhysChem*, 2016, **17**, 2824–2838.
48 I. Lednev, T.-Q. Ye, P. Matousek, M. Towrie, P. Foggi, F. Neuwahl, S. Umapathy, R. Hester and J. Moore, *Chem. Phys. Lett.*, 1998, **290**, 68–74.
49 R. W. Hendler and R. I. Shrager, *J. Biochem. Biophys. Methods*, 1994, **28**, 1–33.
50 I. H. M. van Stokkum, D. S. Larsen and R. van Grondelle, *Biochim. Biophys. Acta, Bioenerg.*, 2004, **1657**, 82–104.
51 T. Nagele, R. Hoche, W. Zinth and J. Wachtveitl, *Chem. Phys. Lett.*, 1997, **272**, 489–495.
52 J. Azuma, N. Tamai, A. Shishido and T. Ikeda, *Chem. Phys. Lett.*, 1998, **288**, 77–82.
53 F. Aleotti, L. Soprani, A. Nenov, R. Berardi, A. Arcioni, C. Zannoni and M. Garavelli, *J. Chem. Theory Comput.*, 2019, **15**, 6813–6823.
54 I. Conti, M. Garavelli and G. Orlandi, *J. Am. Chem. Soc.*, 2008, **130**, 5216–5230.
55 Y. Lu, E. Diau and H. Rau, *J. Phys. Chem. A*, 2005, **109**, 2090–2099.
56 S. Yuan, Y. Dou, W. Wu, Y. Hu and J. Zhao, *J. Phys. Chem. A*, 2008, **112**, 13326–13334.
57 J. Bahrenburg, F. Renth, F. Temps, F. Plamper and W. Richtering, *Phys. Chem. Chem. Phys.*, 2014, **16**, 11549–11554.
58 M. Boggio-Pasqua, M. Ravaglia, M. J. Bearpark, M. Garavelli and M. A. Robb, *J. Phys. Chem. A*, 2003, **107**, 11139–11152.
59 R. S. H. Liu and G. S. Hammond, *Photochem. Photobiol. Sci.*, 2003, **2**, 835–844.